

Observations of Flexure and the Rheology of the Oceanic Lithosphere

J. H. BODINE, M. S. STECKLER, AND A. B. WATTS

Lamont-Doherty Geological Observatory and Department of Geological Sciences of Columbia University, Palisades, New York 10964

Observations of flexure indicate that the effective flexural rigidity of oceanic lithosphere is a function of the age of the lithosphere at the time of loading, and hence temperature. We have used a yield stress envelope model constrained by data from experimental rock mechanics to determine how the flexural parameters and rheologic properties of oceanic lithosphere are related. The results of our model for seamounts and oceanic island loads in the interior of plates suggest that following loading, rapid stress relaxation occurs as the plate 'thins' from its short-term to its long-term ($>10^6$ years) mechanical thickness. The mechanical thickness, which determines the effective flexural rigidity of the plate, is strongly dependent on temperature and weakly dependent on load size and duration ($>1-10$ m.y.). The results of our model for convergent plate boundaries suggest that changes in the shape of the Outer Rise along an individual trench system may be due to variations in the horizontal load acting across the boundary (<1 kbar). The model predicts a narrow zone of high strain accumulation seaward of a trench which is in agreement with variations in crustal velocities and seismicity patterns observed along some trench systems.

INTRODUCTION

The apparent rigid translations of the lithospheric plates together with the support of large surface loads for long periods of time require the existence of a strong lithosphere overlying a weak asthenosphere. Geological and geophysical observations indicate the oceanic lithosphere is strong and responds to horizontal and vertical forces by bending. These observations include the existence of an Outer Rise seaward of trenches [Hanks, 1971; Watts and Talwani, 1974], distinct zones of seismic activity in the subducting plate [Hasegawa *et al.*, 1977; Engdahl and Scholz, 1977; Chen and Forsyth, 1978; Chapple and Forsyth, 1979], and directly observed or inferred vertical motions and deflections of the lithosphere related to surface loads [Vening-Meinesz, 1941; Walcott, 1970; Watts and Cochran, 1974; McNutt and Menard, 1978].

Although the importance of a strong lithosphere has been recognized for a number of years [Barrell, 1914; Gunn, 1944; Vening-Meinesz, 1941], precisely how the strength of the lithosphere varies through its thickness has not been well known. Simple elastic, viscous, visco-elastic, and elastic-plastic models have been developed to approximate the mechanical properties of the lithosphere [Walcott, 1970; DeBremaecker, 1977; McAdoo *et al.*, 1978]. More recently it has become possible to include improved constraints on the rheology of the lithosphere and to construct more accurate models.

Despite the simplicity of the elastic model, it has been used successfully to explain a wide range of geological and geophysical observations [Hanks, 1971; Watts and Cochran, 1974; Dubois *et al.*, 1975; McNutt and Menard, 1978; Watts, 1978]. An important result of these studies is that the effective flexural rigidity of the oceanic lithosphere increases with age [Watts *et al.*, 1980a, b]. This relationship suggests that the effective flexural rigidity is predominantly determined by the temperature structure of the lithosphere. The elastic model provides, however, only a first-order approximation of the mechanical properties of the lithosphere. Effective elastic thicknesses which can explain observations, for example, are a factor of 2 or 3 smaller than the thermal or the seismic thickness of the lithosphere. It is thus not clear how the effective elastic thickness, as determined from the effective flexural rigidity, is related to the actual lithosphere.

The recent progress in understanding the material properties of olivine provides a basis for improving the simple mechanical models [Goetze and Brace, 1972; Kohlstedt and Goetze, 1974; Weertman and Weertman, 1975; Kohlstedt *et al.*, 1976]. Experimental results are now available for rock deformation at pressures and temperatures appropriate for the crust and uppermost mantle. With assumptions of the variation of temperature and pressure with depth, these results can be extrapolated to geologic strain rates. This information has been used to map deformation zones in the lithosphere [Stocker and Ashby, 1973; Ashby and Verrall, 1978; Goetze, 1978; Goetze and Evans, 1979]. Ductile deformation is predicted in the lower lithosphere, where temperature and pressures are high. The effective creep mechanism controlling ductile flow in this region is determined by strain rate and applied shear stress. At shallower depths, where temperatures are lower, deformation occurs by brittle fracture or frictional sliding.

The overall objective of this paper is to determine how the flexural parameters and the rheologic properties of the oceanic lithosphere are related. We first briefly review the observations of flexure. We then construct a rheological model of the oceanic lithosphere based on results of experimental rock mechanics. This model is used to calculate continuous deflection profiles which are then compared to the observations of flexure.

OBSERVATIONS OF FLEXURE

We summarize the results of oceanic plate flexure in Figure 1. This figure is similar to recent compilations by Watts *et al.* [1980a, b] but differs in that a relaxed [Anderson and Minster, 1980] rather than the seismic value of Young's modulus is used to calculate the effective elastic thickness T_e (see the notation section at the end of the paper). The results for mid-ocean ridges (squares) and seamounts and oceanic islands (circles) have generally been determined by comparing the relation between observed gravity anomalies and bathymetry to theoretical models. The results for the Outer Rise seaward of trenches (triangles) are based mainly on the comparison of observed bathymetry to deflections of a theoretical model.

The age plotted on the horizontal axis in Figure 1 is the age of the oceanic lithosphere at the time it is loaded. For example, the age plotted for an 80-m.y.-old seamount on 150-

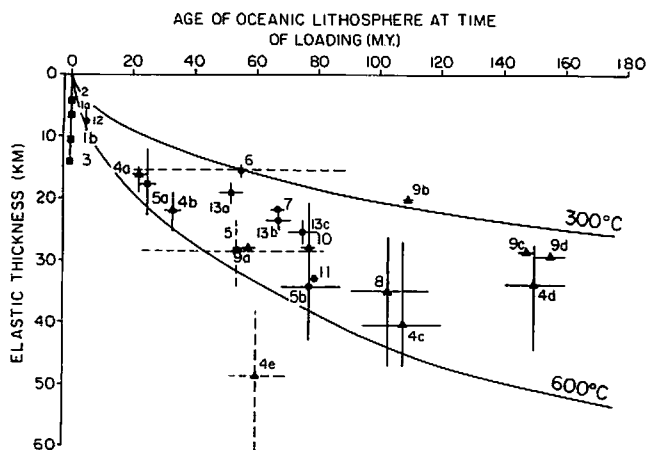


Fig. 1. Plot of T_e , the effective elastic thickness of the oceanic lithosphere, against age of the lithosphere at the time of loading: 1, East Pacific rise crest [Cochran, 1979]; 2, Juan da Fuca rise crest [McNutt, 1979]; 3, Mid-Atlantic ridge crest and flank [McKenzie and Bowin, 1976]; 4, Deep-sea trench-outer rise systems [Caldwell, 1979]; 4a, Nankai trough; 4b, Middle America trench; 4c, Kuril trench; 4d, Mariana trench; 4e, Aleutian trench; 5, Hawaiian-Emperor seamount chain [Watts, 1978]; 5a, Emperor seamounts north of 40°N; 5b, Hawaiian ridge and Emperor seamounts south of 40°N; 6, Pacific ocean atolls from the Cook-Austral, Tuamotu, and Pitcairn island groups [McNutt and Menard, 1978]; 7, Great Meteor seamount [Watts et al., 1975]; 8, Kuril trench [McAdoo et al., 1978]; 9, Deep-sea trench-outer rise systems [Caldwell et al., 1976]; 9a, Aleutian trench; 9b, Kuril trench; 9c, Bonin trench; 9d, Mariana trench; 10, Hawaiian ridge [Suyenaga, 1977]; 11, Hawaiian ridge [Walcott, 1970]; 12, Walvis ridge [Detrick and Watts, 1979]; 13, Pacific oceanic islands [Cazenave et al., 1980]; 13a, Marqueses Island; 13b, Society Islands; 13c, Crozet Island. Symbols indicate ridge crest (squares), seamounts and oceanic islands (circles), and deep-sea trench outer rise systems (triangles). Dashed lines indicate either studies based on a wide range of ages (5, 6) or uncertain values (4e). The elastic thickness has been computed assuming Young's modulus $E = 6.5 \times 10^{10}$ N/m². The 300°C and 600°C oceanic isotherms are based on the cooling plate model of Parsons and Sclater [1977].

m.y.-old seafloor would be 70 m.y. For bending seaward of trenches the current age of the subducting plate is used. The durations of the seamount and island loads plotted in Figure 1 are in the range of 2 to 55 m.y. Figure 1 therefore suggests that the initial response of the oceanic lithosphere to loading is effectively 'frozen in' with little or no relaxation on these time scales.

Figure 1 shows that the estimates of T_e for ages greater than 80 m.y. are based only on Outer Rise bathymetry. These estimates may be uncertain for two main reasons. First, the low-amplitude (200–500 m) and the relatively long wavelength (200–400 km) of the Outer Rise make accurate determinations of its shape and the unflexed or reference depth difficult. Second and perhaps more important is the possible influence of horizontal boundary forces. Variations of the Outer Rise shape in many trench systems require large changes in the effective flexural rigidity along the strike of the trench if explained with the elastic model [Bodine and Watts, 1979]. An elastic-plastic model in which yielding occurs can, however, explain the Outer Rise without requiring large changes in rigidity. In this model horizontal boundary forces can cause variations in the amount of yielding and in the Outer Rise shape.

The estimates in Figure 1 therefore represent the best available evidence of the variation of T_e with age. These estimates, however, are mainly based on the simple elastic model, and it

is not clear how they are related to the actual rheological properties of the oceanic lithosphere.

A RHEOLOGICAL MODEL OF THE OCEANIC LITHOSPHERE

We have constructed a rheological model of the lithosphere which satisfies the constraints of experimental rock mechanics. The model is based on the rheology proposed by Goetze and Evans [1979] using the deformation laws of olivine discussed by Goetze [1978]. These flow laws govern the transition between elastic and perfectly plastic deformation in the model. The resulting elastic-plastic yield envelope in which yielding is due to deviatoric stresses in the plane of bending is shown in Figure 2.

The yield envelope contains three principal deformation regions. At shallow depths, pressure effects on yield strength dominate, and yielding occurs as cataclastic flow described by the Coulomb frictional sliding criteria. Deformation in this region is relatively insensitive to temperature variations, strain rate, and rock type. At greater depths, temperature effects become dominant, and thermally activated creep mechanisms [Goetze, 1978] govern the yield strength and the shape of the yield envelope. Power law creep is dominant for shear stresses less than 2 kbar and is expressed as

$$\dot{\epsilon} = 70 \sigma^3 \exp \{-Q_p/RT\} \quad (1)$$

where $\dot{\epsilon}$ is strain rate (s⁻¹), σ , is shear stress (bars), T is temperature (°K), and R is the universal gas constant. At shear

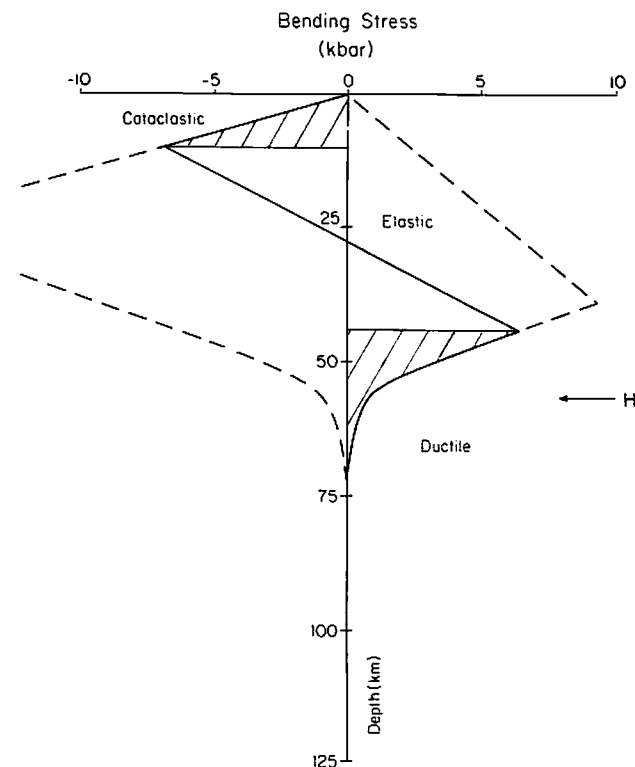


Fig. 2. The yield envelope for the elastic-plastic plate model is constrained by pressure-dependent cataclastic flow mechanisms at shallow depths and empirically determined thermally activated creep laws for the lower part of the lithosphere. Strain rate must be assumed and temperature structure is estimated from the cooling plate model of Parsons and Sclater [1977]. Plate deformation is elastic in the parts of the plate where bending stresses do not exceed the yield stress. The mechanical thickness H is defined as the depth below which the shear strength of the plate is less than 500 bars.

stresses greater than 2 kbar, power law creep breaks down, and a better relation is given by the Dorn law,

$$\dot{\epsilon} = 5.7 \times 10^{11} \exp \left\{ -Q_D/RT (1 - \sigma_s/8.5 \times 10^4)^2 \right\} \quad (2)$$

The activation energies Q_p , Q_D for the two expressions are different to ensure continuity at 2-kbar shear stress. Activation energy values for both 'wet' and 'dry' olivine are summarized in the notation section. Equation (1) shows a strong exponential dependence on temperature resulting in a rapid de-

crease of yield stress with depth. The point at which the ductile yield stress is 500 bar approximately marks the transition from high to low shear strength and is indicated in Figure 2 as the 'mechanical thickness' H of the lithosphere.

In order to apply (1) and (2) to the oceanic lithosphere, we specified the temperature distribution with depth using the cooling plate model of *Parsons and Sclater* [1977]. In Figure 3a the yield envelope for 80-m.y. oceanic lithosphere is shown for several different strain rates. The mechanical thickness is large for high strain rates such as those that may be associated with short-duration seismic waves or glacial rebound. For the low strain rates that may be associated with geological processes such as seamount loading and sedimentary basin formation, the mechanical thickness is much smaller. Thus Figure 3a suggests that for loads of short duration the lithosphere appears relatively thick and rigid, while for loads of long duration the part of the lithosphere capable of supporting large stress differences is much thinner. Figure 3b shows the variation of the shape of the yield envelope for different ages of oceanic lithosphere at an assumed strain rate of 10^{-18} s^{-1} . This figure shows that the mechanical thickness increases substantially with age similar to the trend observed in Figure 1.

In order to compare the yield envelope model to the observations of flexure we calculated continuous deflection curves for seamount loads in the interior of plates and for boundary loads at trenches. The model is similar to the elastic-plastic models constructed by *McAdoo et al.* [1978] and *Bodine and Watts* [1979]. The main differences are in the inclusion of a better constrained rheology and the ability to calculate deflections due to distributed loads. The base of the elastic-plastic plate is at a depth that corresponds to the mechanical thickness H . Material at greater depths is considered to be an inviscid fluid. The model is based on thin plate theory and assumes plane strain and small deflections. The details of the formulation of the model for flexure at seamounts and trenches are given in the appendix.

FLEXURE AT SEAMOUNTS

We consider the flexure at seamounts to be caused by a distributed load in the interior of an oceanic plate. The model assumes two-dimensionality which is appropriate to linear geological features such as seamount chains and aseismic ridges. Thus the model is representative of most of the features plotted in Figure 1.

Figure 4 shows the extent of yielding in a continuous plate due to a distributed load. In the peripheral bulge region, where the plate is convex upward, the plate yields more near the top than at the bottom due to the lower brittle shear strength of the plate under tension. Near the center of the deflection, bending stresses are of opposite sign, and the maximum yielding occurs at the bottom of the plate. The strains developed during bending can be estimated from the model.

The deflection curve and the estimate of strain under the load are determined by the assumed strain rate. By relating strain and strain rate for several deflection curves we can calculate an absolute time for each assumed strain rate (Tables 1 and 2). This relation allows the deflection curve to be determined as a function of time since the formation of the load. This is illustrated in Figure 5, where deflections beneath an instantaneously applied seamount load (approximating the size of Oahu island in the Hawaiian ridge) are plotted for a range of load duration, $t = 0$ to 10^8 year (Table 1). At $t = 0$ the entire thickness of the thermal lithosphere remains elastic.

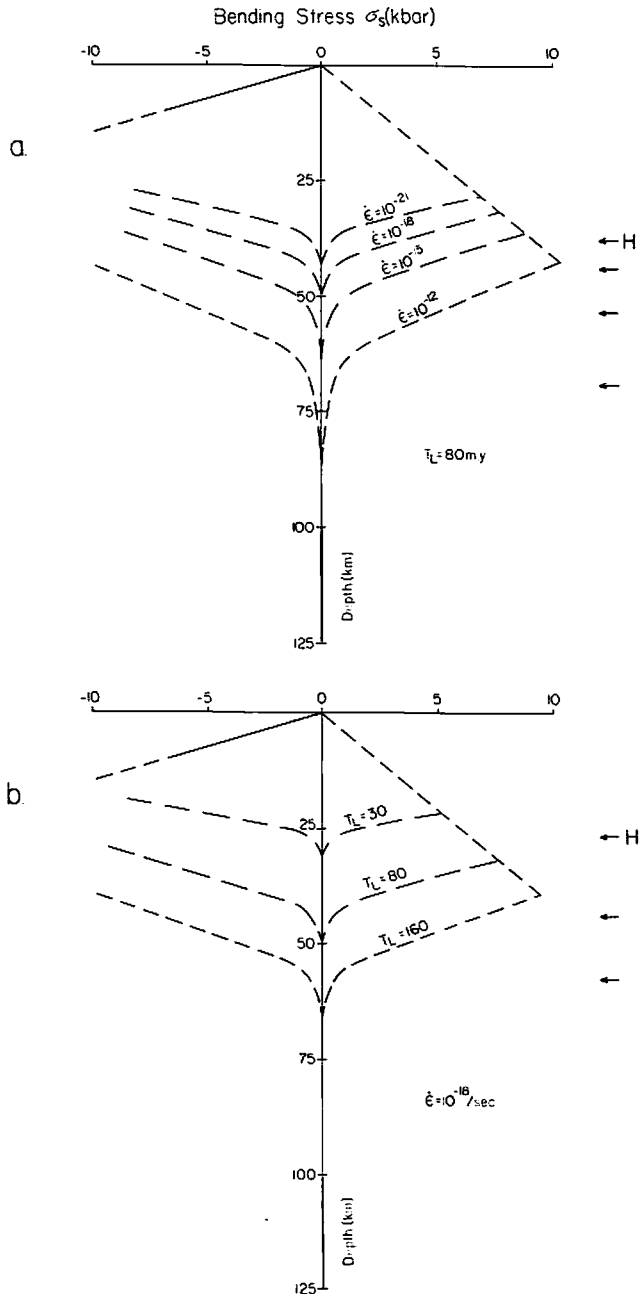


Fig. 3. (a) The effects on the yield envelope of varying assumed strain rate and (b) assumed plate age or temperature structure are shown. High strain rates such as due to short-term seismic loads result in a large mechanical thickness. For lower strain rates which might be associated with longer term geologic processes, the mechanical thickness is significantly thinner. Changes in temperature structure are seen to have an even larger effect on the mechanical thickness. The increase in mechanical thickness with age suggests a similar relation for the effective rigidity of the plate.

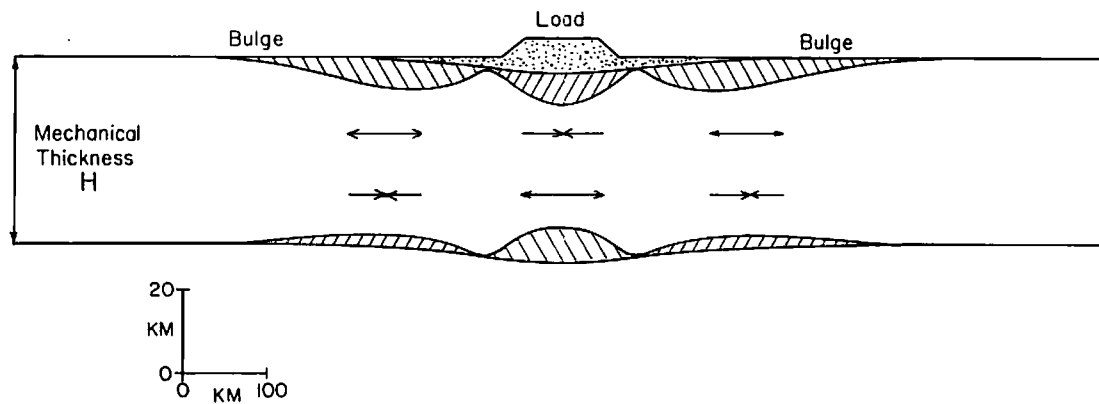


Fig. 4. A continuous deflection profile is produced using the yield envelope rheology. The load approximates the island of Oahu in the Hawaiian island chain on an 80-m.y.-old plate with assumed strain rate of 10^{-18} s^{-1} . The hatched regions indicate the extent of plastic yielding due to tensile and compressive bending stresses. H is the mechanical thickness.

The asthenosphere below the thermal thickness of the lithosphere is assumed in the model to be inviscid. Postglacial rebound studies (for example, *Walcott* [1972]), however, indicate a nonzero viscosity for the asthenosphere but only for load durations $\geq 10^5$ years. The model results show that the mechanical thickness initially thins rapidly with time, resulting in a shorter-wavelength, larger-amplitude deflection. At longer times, the rate of thinning decreases. Thus the model predicts rapid relaxation for load durations of less than 1 to 10 m.y. and little subsequent change in the deflection shape for longer times.

The rapid relaxation following loading will result in subsidence beneath and adjacent to the load. Thus we may expect evidence of relaxation and subsidence at Hawaii island, which is younger than 0.4 m.y. [*McDougall and Swanson*, 1972]. *Endo and Rogers* [1981] have shown from composite focal mechanism solutions based on 60 earthquakes that a distinct and well-defined radial pattern of the maximum compressive axes exists beneath the island. Although they did not prefer a continuous plate model, the radial pattern is evidence for currently active plate relaxation. Archaeological data [*Apple and MacDonald*, 1966] indicate that Hawaii is subsiding, and tide gauge data [*Moore*, 1970] indicates subsidence rates of 4.1 mm/yr relative to Oahu. Although a large part of the subsidence can be attributed to the transfer of volcanic material from beneath the island [*Moore*, 1970; *Swanson*, 1972], we estimate that the transfer rate of this material ($\sim 9 \times 10^6 \text{ m}^3/$

month; *Swanson* [1972]) cannot fully account for the subsidence rates that are observed. The remaining subsidence may be attributed to relaxation of the lithosphere beneath the island.

The gravity anomaly is sensitive to both the load and the resulting deflection of the lithosphere. The variations in deflections shown in Figure 5 suggest that the free-air gravity anomaly would also change rapidly immediately following loading but would not be expected to change significantly for times greater than 1 to 10 m.y. Figure 6 shows the computed gravity anomaly profiles based on our model deflections for two different age loads in the Hawaiian-Emperor seamount chain (Oahu, 3 m.y.; Nin Toko, 52 m.y. [*McDougall and Azizur-Rahman*, 1972; *Clague and Jarrard*, 1973, Figure 5]). The gravity anomaly was computed for the case immediately after emplacement of the loads and for durations corresponding to the age of each load. Although the gravity anomaly for $t = 0$ differs from the observed anomalies for both loads, the gravity anomalies for $t = 3$ and $t = 52$ m.y. are similar in shape to the observed anomalies. Figure 6 therefore shows that gravity anomalies calculated from the model results for long-term loads are consistent with observed gravity data.

The mechanical properties of the oceanic lithosphere predicted by the model are thus consistent with observations for seamount loads. Rapid stress relaxation following load emplacement results in a decrease in effective rigidity with increasing load duration. As bending stresses relax at depth and

TABLE 1. Model Results for a Seamount Load in the Interior of the Plate

$\dot{\epsilon}$, s^{-1}	H , km	σ_4 , bars/m	M , $\times 10^{18} \text{ N}$	ζ_1 , km	ζ_2 , km	ζ_N , km	w'' , $\times 10^{-6} \text{ m}^{-1}$	ϵ , %	w_0 , m	t , years
1.16×10^{-8}	104.3	-0.117	1.9853	3.18	88.46	48.67	0.0719	0.3497	2198	4.65×10^{-4}
1.16×10^{-9}	88.7	-0.153	1.1615	3.74	74.45	41.42	0.1018	0.4219	2488	5.21×10^{-3}
1.16×10^{-10}	82.3	-0.172	0.9066	4.04	68.65	38.45	0.1198	0.4605	2634	5.84×10^{-2}
1.16×10^{-12}	70.0	-0.250	0.5335	4.81	58.51	33.11	0.1723	0.5705	2988	7.34
1.16×10^{-13}	63.0	-0.308	0.3799	5.27	52.62	30.04	0.2146	0.6446	3216	8.23×10^1
1.16×10^{-14}	58.0	-0.354	0.2946	5.37	48.09	27.79	0.2613	0.7261	3428	9.23×10^2
1.16×10^{-15}	53.8	-0.370	0.2392	6.11	43.72	25.73	0.3138	0.8074	3659	1.03×10^4
1.16×10^{-16}	50.3	-0.412	0.1987	6.43	40.66	24.20	0.3641	0.8809	3853	1.16×10^5
1.16×10^{-17}	47.2	-0.448	0.1692	6.80	37.75	22.80	0.4266	0.9727	4057	1.30×10^6
1.16×10^{-18}	44.6	-0.501	0.1442	6.87	35.97	21.75	0.4557	0.9912	4209	1.46×10^7
1.16×10^{-19}	42.1	-0.553	0.1248	6.93	33.79	20.63	0.5042	1.3990	4384	1.63×10^8

The values on this table are for deflections under a load approximating Oahu. The mechanical thickness (H) and slope of the bottom of the yield envelope (σ_4) are determined by the assumed plate age (80 m.y.) and the strain rate ($\dot{\epsilon}$). Deflection parameters are measured at $x = 0$ directly beneath the load. M , bending moment; ζ_1 , ζ_2 , ζ_N , top, bottom, and neutral surface of the elastic core; w'' , curvature; ϵ , strain at the top of the plate; w_0 , deflection amplitude.

TABLE 2. Relation of ϵ and $\dot{\epsilon}$ to Time

Age, m.y.	<i>a</i>	<i>b</i>	<i>cc</i>	<i>A</i>	<i>B</i>
<i>Oahu, Hawaiian Chain</i>					
50	-20.89	-128.8	0.990	3.205×10^{-3}	4.568×10^{-2}
80	-20.16	-131.7	0.991	2.289×10^{-3}	4.726×10^{-2}
160	-27.28	-176.4	0.998	2.200×10^{-3}	3.536×10^{-2}
<i>Nin Toku, Emperor Chain</i>					
50	-18.92	-138.0	0.995	1.139×10^{-3}	5.020×10^{-2}
80	-21.75	-160.7	0.997	0.982×10^{-3}	4.396×10^{-2}
160	-28.06	-206.7	0.999	0.915×10^{-3}	3.441×10^{-2}

Correlation coefficient is shown by *cc*; $\ln \dot{\epsilon} = a \ln \epsilon + b$; $\epsilon = At^B$; $\dot{\epsilon} = ABt^{B-1}$. The coefficients relating strain (ϵ) and strain rate ($\dot{\epsilon}$) are calculated using a linear regression fit to logs of ϵ , and $\dot{\epsilon}$ values from Table 1.

concentrate in the upper cooler part of the lithosphere, the long-term response of the plate becomes frozen in for times greater than 1 to 10 m.y.

FLEXURE SEAWARD OF TRENCHES

We consider flexure seaward of trenches to be due to boundary forces associated with the subduction of the lithosphere. In our model the flexure is produced by a bending moment determined from the amplitude and wavelength of the Outer Rise. We also are able to apply horizontal compressive or tensile forces acting across the trench.

Figure 7a shows the extent of yielding for an oceanic plate at a trench. We estimated a strain rate from the strain developed during flexure and the convergence rate across the trench. Far from the trench, where the deflections are small, the plate is assumed to remain entirely elastic. At x_{11} (Figure 7 and the appendix), elastic-plastic rheology becomes effective and the plate begins to yield with bending. Tension develops in the top of the plate and compression at the bottom until unbending begins at x_{12} (appendix). Larger applied bending moments result in more yielding and a lower effective rigidity.

The effects of applied horizontal forces (tension or compression) are shown in Figure 7b. With the application of a horizontal force the deflection is greater, the apparent wavelength of the Outer Rise is smaller, and yielding is more extensive. In addition, the horizontal forces result in a thinning of the elastic core seaward of x_{11} where bending is negligible, resulting in a reduction of the effective rigidity of the plate.

Although horizontal compression had a greater effect, both tension and compression resulted in greater curvatures in the deflection shape. The differences in deflection due to compression and tension are model dependent, however, and we therefore do not distinguish the sign of the horizontal forces existing across the trench.

We compare the model results to observed bathymetry profiles of the Kuril and Peru-Chile trenches in Figure 8. Each profile was corrected for sediment loading by backstripping and for tilting due to lithospheric cooling. Variations in the shape of the Outer Rise along these trenches are similar to those described for the Izu-Bonin-Mariana trenches [Bodine and Watts, 1979]. The horizontal loads required for the model to fit these observed deflections are much less than those required by previous elastic-plastic model studies (≤ 1.0 kbar compared to 2.0–6.0 kbar).

These studies suggest that variations in the horizontal load along the trench are of the order of hundreds of bars. We have shown by using the yield envelope model that horizontal loads required to explain observations of flexure are 1 kbar or less. These stress estimates, although higher than stress drops associated with earthquakes, are based on models which incorporate estimates of the strength of rocks inferred from experimental rock mechanics.

RESULTS

We have so far compared the model results to geophysical observations at specific features on the ocean floor. In this section we examine the general behavior of the model for a range of loading conditions and ages of oceanic lithosphere.

In Figure 9 we compare the estimates of effective elastic thickness T_e for seamount loads to the model results. The equivalent elastic thickness for the model results was determined by best fitting the amplitude and wavelength of the model deflection to that of the simple elastic model. Figure 9 shows the equivalent elastic thickness for both large and small loads (Oahu and Nin Toku, Figure 6). For each case, results were obtained for the load durations ranging from 1 to 100 m.y. Figure 9 shows that the equivalent elastic thickness does not depend significantly on load size and that it does not change appreciably after the initial rapid relaxation. The main result shown is that the equivalent elastic thickness is strongly dependent on the age of the oceanic lithosphere at

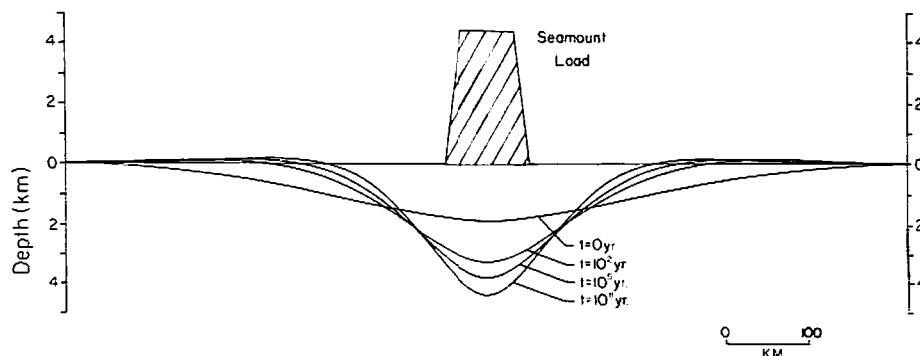


Fig. 5. A deflection that corresponds to a given strain rate may be considered an equilibrium configuration for the lithosphere at a discrete point in time following load emplacement. Using model deflection results under a constant seamount load for several assumed strain rates, strain beneath the load can be calculated. Deflection shape may then be estimated as a function of time. For a load approximating the size of Oahu ($\rho_L = 2.6 \text{ g/cm}^3$) it is seen that deflection shape initially changes very rapidly with increasing time or duration of the load. At $t = 0$ the entire thickness of the thermal lithosphere (125 km) remains elastic. Deflections vary from a long-wavelength, rigid initial response to a shorter-wavelength, lower-rigidity configuration. For load durations greater than about 1–10 m.y. the deflection shape changes very little.

Hawaiian-Emperor Seamount Chain

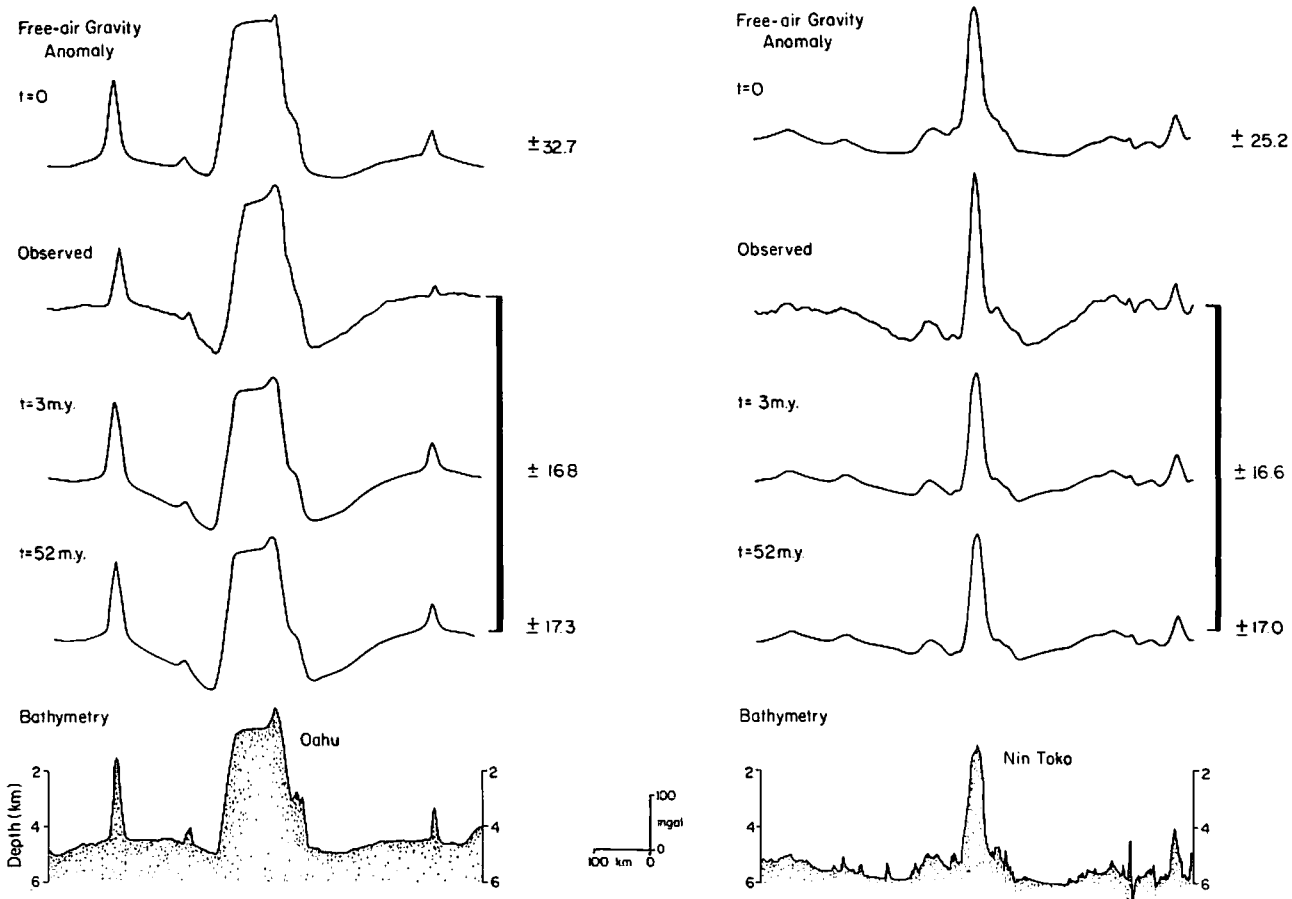


Fig. 6. A comparison of calculated and observed gravity anomalies for different assumed load durations and resulting deflections beneath the observed bathymetric loads of Oahu and Nin Toko is shown. The rms differences between calculated and observed gravity anomalies are listed beside each profile. For a very short load duration the wavelength of the calculated gravity anomalies is too large. For 3 m.y. and 52 m.y. the calculated and observed anomalies are very similar, indicating that the long-term deflection configuration has been reached by at least $t \approx 3$ m.y.

the time it is loaded. However, the effective elastic thicknesses for our assumed rheology are too large (Figure 9). The fit of the models to observations may be improved by varying the assumed rheology.

In our model we have used experimental results of Goetze [1978] derived from the deformation of dry, single crystals of olivine. The experimental results of Post [1977], however, indicate that there may be significant differences in strength between wet and dry dunite. The water available in hydrated dunite may facilitate movement of the rate limiting species, probably oxygen atoms, and thus permit easier movement of dislocations. The effect of water can be expressed as a lower activation energy in (1) and (2) [Post, 1977]. The amount of water in the mantle, however, is poorly known. We found (Figure 9) that values of the activation energy intermediate between those of Goetze [1978] and Post [1977] best fit the observations.

We have not included other factors which may affect the rheological properties of the lithosphere. For example, there may be significant differences in the creep strength of rocks indicated from single-crystal experiments [Kohlstedt and Goetze, 1974] and those using polycrystalline aggregates [Post, 1977]. There is controversy, however, regarding the influence of the mechanical apparatus used in these experiments, and it

is not clear what mechanism might explain the difference in strength. The strength of rocks is also dependent on the effects of pore pressure [Brace and Kohlstedt, 1980]. Results from conductivity and permeability studies indicate water-filled pores may exist in crustal rocks to depths of greater than 8 km. The presence of water would effectively weaken the upper part of the plate [Brace and Kohlstedt, 1980]. We have limited our model to flow laws appropriate to most experimental results. At large strains and stresses other deformation mechanisms such as ductile faulting [Post, 1977] may become more important. Although the laws by which ductile faulting might occur are not well known, it is clear that the effect would be to weaken the plate. These modifications to our assumed rheology would generally act to weaken the plate. Thus although our model is probably biased toward larger rigidities, the conclusions drawn from Figure 9 would not change.

We have assumed in our calculations a uniform temperature structure for oceanic lithosphere based on the cooling plate model. We have therefore not included perturbations of the temperature structure of the lithosphere which may arise from volcanism. Since many seamounts and oceanic islands are formed above hot spots, it has been suggested that their emplacement is accompanied by substantial reheating of the lithosphere [Detrick and Crough, 1978]. Based on the sub-

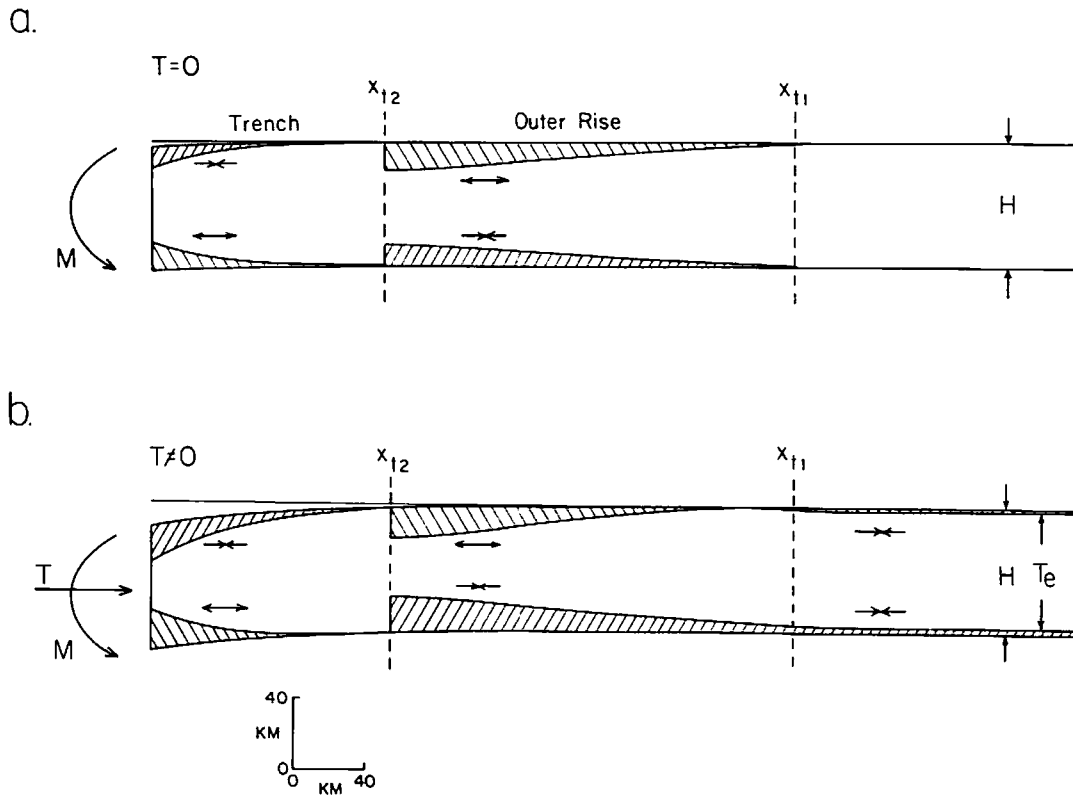


Fig. 7. For bending seaward of trenches a constant strain rate related to the subduction rate is assumed. Figure 7a shows the extent of plastic yielding for a plate with no horizontal loading ($T = 0$); x_{11} and x_{12} are the points at which plastic yielding first begins and where unbending occurs, respectively. As unbending begins, the plate is momentarily entirely elastic before yielding again with stresses of opposite sign. The effects of an applied horizontal load (compressive in this example) are shown in Figure 7b. The loading produces an initial thinning in the undeflected part of the lithosphere distant from the trench, resulting in greater plastic yielding and a decrease in the apparent wavelength of the deflection.

sidence of atolls and guyots and the height of associated topographic swells, *Detrick and Crough* [1978] have suggested that the thermal age of the lithosphere is reset to 30 m.y. during volcanism.

The results illustrated in Figure 9, however, indicate that if reheating has occurred, it apparently has not affected the temperature structure of the mechanical layer. Conductive heating alone can produce topographic uplifts [*Crough and Thompson*, 1976]. However, if for example, the Hawaiian Swell formed in 3 m.y. [*Detrick and Crough*, 1978, p. 1242], then the transfer of heat by conduction would be too slow to explain the rate of uplift [*Crough and Thompson*, 1976; *Gass et al.*, 1977]. Convective heat transfer in which basal heating rapidly elevates temperatures at depth has been proposed as an alternative mechanism [*Detrick and Crough*, 1978; *Withjack*, 1979]. While this heat transfer mechanism can result in a large change in the average temperature structure, significant heating would only occur in the lower part of the lithosphere. Thus the upper mechanical layer would remain relatively unaffected, and the results shown in Figure 9 would be unaltered.

In Figure 10 we compare estimates of effective elastic thickness T_e for bending at trenches to the model results. We determined the equivalent elastic thickness for the model results using the range of applied bending moments which correspond to amplitudes of the Outer Rise, w_b , of 200 to 400 m. Figure 10 clearly shows the trend of increasing equivalent elastic thickness with increasing age of the plate. As in Figure 9, consideration of a wet rheology resulted in a weaker plate

and a better overall fit to the observations. The data points departing from this trend (4d, 9b–9d) can be explained by the model with application of horizontal boundary loads of no greater than 1 kbar (dashed lines). Thus the changes in the overall shape of the Outer Rise along an individual trench system can be explained by small variations in horizontal loads (≤ 1 kbar) and do not require large changes in the mechanical properties of the oceanic lithosphere.

The large curvatures observed along some trench systems (Figure 8; *Bodine and Watts* [1979]) suggest that high strains are developed during bending at trenches. Such high strains, particularly if they are associated with brittle deformation, may be related to the distribution of seismicity. Figure 11 is a plot of hypocenter depths for seismic events seaward of trenches from a compilation by *Chapple and Forsyth* [1979]. This plot shows the vertical zonation of focal mechanism solutions for seismic events from different trench systems. Many of the deepest tensile events correspond to sites at trenches where the largest horizontal boundary forces (tensile or compressive) are required to explain the shape of the Outer Rise. We show in Figure 11 the range of neutral surface depths (hatching) based on our model ($w_b = 200$ to 400 m) with applied tension (lower bound, ≥ -1 kbar) and compression (upper bound, ≤ 1 kbar). The aseismic zone between the tensile and compressive regimes is seen to correspond well to the position of the neutral surface of our model. It is probable that the observed earthquakes occur near the upper and lower bounds of the elastic core which surrounds the neutral surface. Although a lowering of the neutral surface (tension) may be preferred in

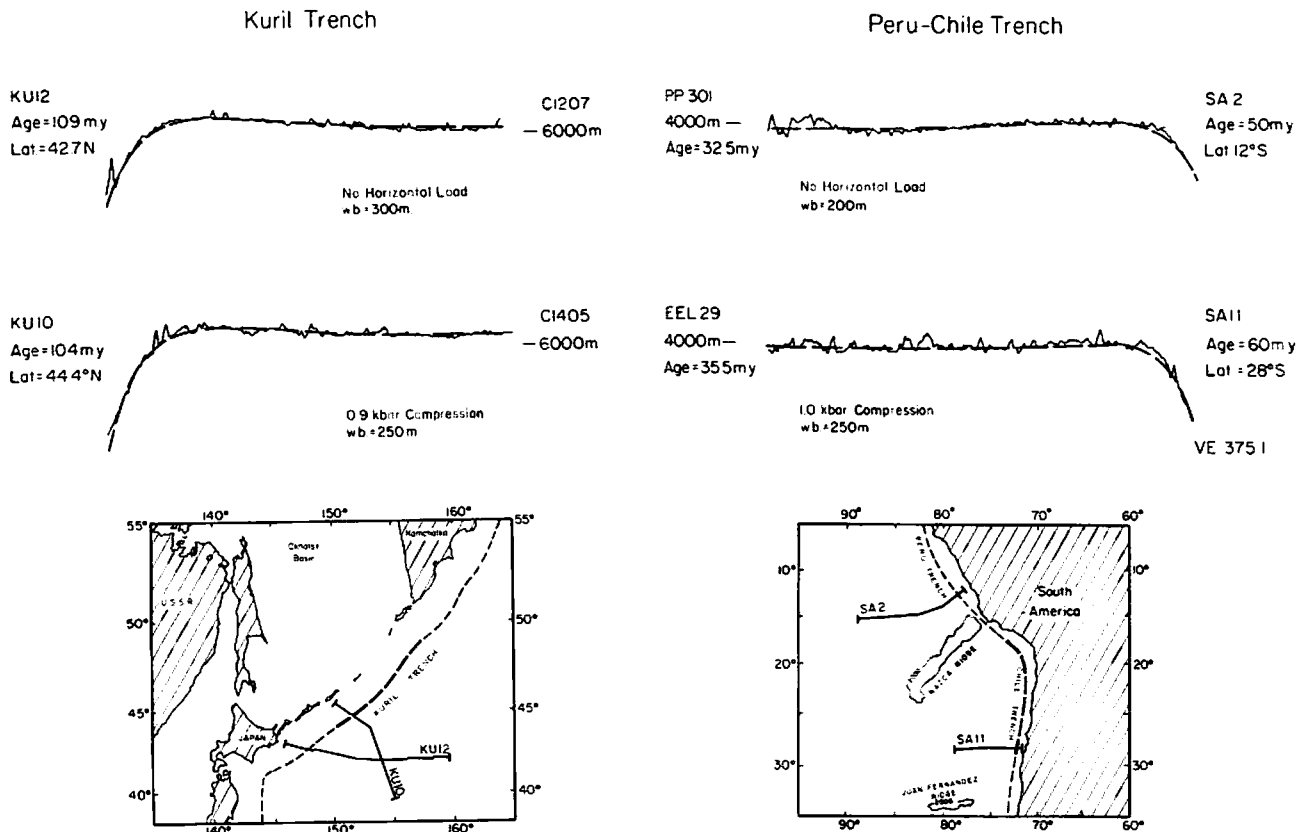


Fig. 8. Comparison of model results for bending at trenches to profiles of the Kuril and Peru-Chile trench systems. Age of the subducting plate is estimated from magnetic lineations, and a strain rate of 10^{-15} s^{-1} is assumed. Heavy lines along the trench axis indicate the zones of steepening of the seaward trench wall, deepening of the trench, and a relative decrease in the estimated wavelength of the Outer Rise. Model deflections can explain the observed Outer Rise shapes along the lightly dashed regions of the trench axes with no horizontal loading. Horizontal loading of up to 1.0 kbar is required to explain Outer Rise bathymetry along the steepened parts of the trench axes.

Figure 11, the nature of the boundary forces at trenches still cannot be easily resolved.

Figure 12 shows that the zone in which strain accumulates is narrow with respect to the wavelength of the Outer Rise. To examine the effects of this concentration of strain, we have matched an observed bathymetry profile of the Izu-Bonin Trench with a model deflection for a plate age of 140 m.y. and a horizontal compressive stress of 1 kbar. The narrow zone of strain accumulation corresponds with a clustering of the seismic events from Figure 11 and changes of the crustal velocities on the seaward wall of the trench. The model is thus consistent with the horizontal and vertical distribution of seismicity and suggests that high strains due to bending may alter the velocity structure of the oceanic lithosphere.

The main results of our study are summarized in Figure 13. Immediately following emplacement of a seamount or ocean island load the oceanic lithosphere relaxes from a short-term to a long-term mechanical thickness. This response to loading is similar to that described by *Anderson and Minster* [1980]. The ability of the yield envelope model to produce continuous deflections due to distributed loads, however, enables us to apply model results directly to observations. The increase in equivalent elastic thickness with age predicted by the model shows the strong influence of temperature structure on the mechanical properties of the oceanic lithosphere. The model results suggest that deflections of the lithosphere are relatively insensitive to load size and to load duration for times greater than 1 to 10 m.y. Thus the results in Figures 9 and 10 indicate

that the simple elastic model can be adequately used to approximate the flexure of the oceanic lithosphere.

CONCLUSIONS

We can make the following conclusions from this study of the observations of flexure and the rheology of the oceanic lithosphere:

1. There is a rapid relaxation of the oceanic lithosphere from the short-term (20–150 s) or seismic thickness to the long-term or mechanical thickness following emplacement of a seamount or oceanic island load. The relaxation occurs by thermally activated creep and results in a concentration of stress in the upper mechanically strong part of the lithosphere.

2. The period of rapid relaxation following loading ($t < 1$ m.y.) is accompanied by a significant decrease in apparent plate rigidity and subsidence of the newly formed feature. Relaxation is essentially complete within 1–10 m.y. following load emplacement. Thus for long-term loads the oceanic lithosphere behaves like an elastic plate.

3. The mechanical thickness of the oceanic lithosphere is a strong function of temperature, and hence the effective flexural rigidity increases with plate age. The equivalent elastic thickness is mainly determined by temperature structure and is relatively insensitive to load size and duration ($t > 1-10$ m.y.).

4. The relation of effective elastic thickness and plate age is complicated near trenches by the possible effects of boundary forces. An increase in the magnitude of horizontal forces

across the trench (tensile or compressive) will decrease the apparent rigidity and effective elastic thickness required to explain the shape of the Outer Rise. Observed deflections at trenches may be explained by horizontal boundary loads of 1 kbar or less. Thus changes in horizontal boundary loads are considered to be a main cause of variations in the shape of the Outer Rise along an individual trench system.

5. High strains may be expected seaward of some trench systems (>5%) with relatively narrow zones of strain accumulation. These zones may be characterized by deep, tensile seismic events and/or an altered crustal velocity structure. Seismic evidence for upper tensile and lower compressive regimes in the lithosphere seaward of trenches may provide information on the nature of horizontal boundary forces (tensile or compressive), although we do not yet feel that they can be distinguished.

6. Considerations of the rheology of the oceanic lithosphere suggest that the simple elastic model is adequate for approximating lithospheric flexure. Based on the rheological constraints used in our model, the effective elastic thickness for loads in the interior of the plate may be approximated by

$$T_e \approx a \cdot \text{age}^{1/2}$$

where $a = 4.3 \pm 0.5$ (dry) and $a = 3.3 \pm 0.5$ (wet). The effective elastic thickness at trenches in the absence of horizontal loading is approximated by

$$T_e \approx a \cdot \text{age}^{1/2}$$

where $a = 4.6 \pm 0.6$ (dry) and $a = 3.6 \pm 0.5$ (wet).

APPENDIX

The differential equation governing deflections for a thin plate is

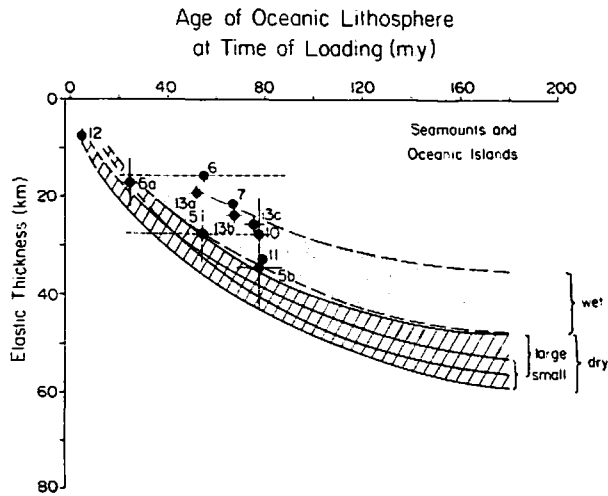


Fig. 9. Comparison of model results for seamount loads to observations for seamounts and oceanic islands from Figure 1. The hatched regions show the range of the 'equivalent' elastic thickness for model deflections due to a small load (Nin Toku, Emperor Chain) and a large load (Oahu, Hawaiian Chain) with load duration of 1 to 100 m.y. The stippled regions are the equivalent elastic thickness range (1- to 100-m.y. load duration) for both loads assuming a wet mantle rheology. The assumption of a wet rheology results in a better overall fit to the observations. The equivalent elastic thickness for the model results does not depend significantly on load size and does not change appreciably for load duration greater than 1 to 10 m.y. The increase of equivalent elastic thickness with age predicted by the model is similar to that of Figure 1.

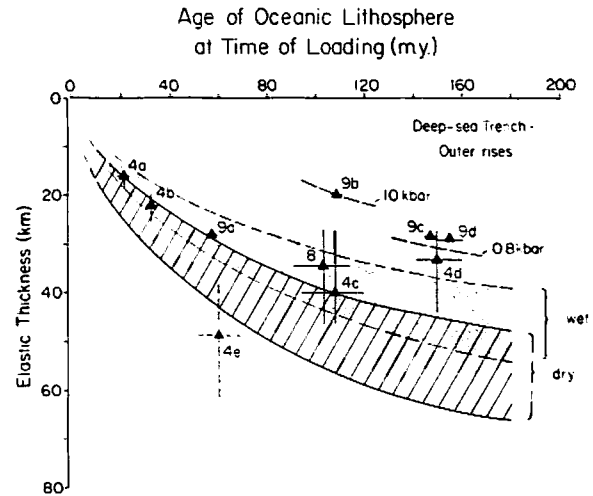


Fig. 10. Comparison of model results for bending at trenches to observations from Figure 1. The hatched region shows the range of equivalent elastic thickness for variations in bending moment corresponding to observed Outer Rise amplitudes of 200-400 m (w_b , see the notation section at the end of the paper). The assumption of a wet rheology results in a better overall fit to the observations. Departures from the trend of increasing elastic thickness with age (9b, 4d, and 9c-9d) can be explained with horizontal loads of 1.0 and 0.8 kbar (dry rheology) applied to the plate (dashed lines).

$$\frac{d^2 M}{dx^2} + T \frac{d^2 w}{dx^2} - kw = 0 \tag{3}$$

where M is the bending moment, T is a horizontal force, w is vertical deflection, and k is the restoring force per unit deflection. For the elastic model the bending moment is linearly related to the curvature by

$$M = -D \frac{d^2 w}{dx^2} \tag{4}$$

where D is the rigidity of the plate (see the notation section) and $d^2 w/dx^2$ is curvature. The bending moment can also be

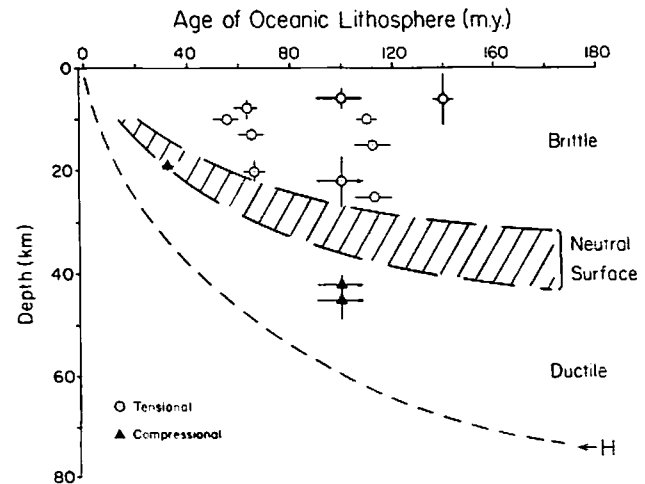


Fig. 11. Comparison of the model results to seismicity patterns seaward of trenches. The open and solid symbols are tensional and compressional events at different trench systems from a summary by *Chapple and Forsyth* [1979]. The range of depths for the neutral surface of our model (for horizontal loading, -1.0 to +1.0 kbar) is located within the aseismic zone between tensile and compressive regimes. Though the neutral surface is significantly lowered when horizontal tension is applied, the available data are not yet sufficient to resolve the sign of the stresses acting across trenches.

Izu-Bonin Trench

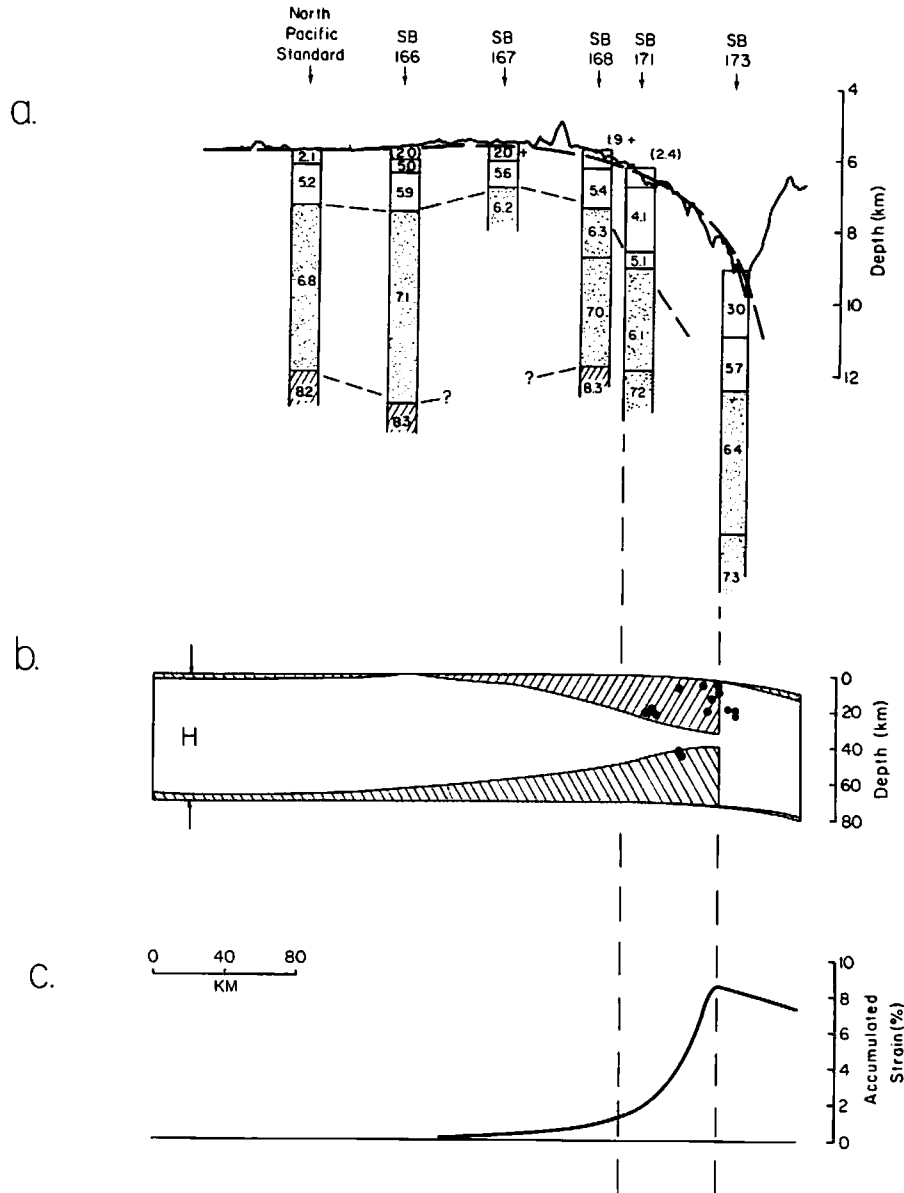


Fig. 12. (a-c) Comparison of an observed bathymetry profile seaward of the Izu-Bonin trench (C2005, latitude $\approx 32^\circ\text{N}$, near IB6 from *Bodine and Watts* [1979]) to the model deflection with a horizontal load of 1.0 kbar (compressive). The calculated strain is for the upper surface of the plate, where brittle deformation occurs by cataclastic flow mechanisms. A zone of anomalous crustal velocity structure based on multichannel seismic reflection profiles and sonobuoy refraction data [*Houtz et al.*, 1980], and a clustering of seismic events (black dots) correlate well with a relatively narrow zone of high strain accumulation near the trench axis.

calculated by integrating over the vertical stress profile of the plate

$$M = \int_{-H/2}^{H/2} \sigma(y)y \, dy \quad (5)$$

$\sigma(y)$ is bending stress as a function of depth, while $H/2$ and $-H/2$ represent the upper and lower bounds of the plate. In the elastic case the stresses vary linearly through the plate. For the elastic-plastic model, however, the vertical stress distribution is not a simple linear function. Those portions of the plate which deform plastically will not sustain stresses greater than the yield stress. From (5) it is thus seen that although stresses

in the yielded parts of the plate contribute to both the bending moment and the rigidity, increases in the bending moment in the elastic-plastic models are limited by the yield criteria. Thus as bending occurs for the elastic-plastic model, the rigidity D in (4) decreases as yielding occurs. The rigidity of the elastic core can be calculated by

$$D_c = \frac{E(\zeta_1 - \zeta_2)^3}{12(1 - \nu^2)} \quad (6)$$

where ζ_1 and ζ_2 are the depth to the top and bottom of the elastic core, respectively. Young's modulus E and Poisson's ratio ν are listed in the notation section. The product of this

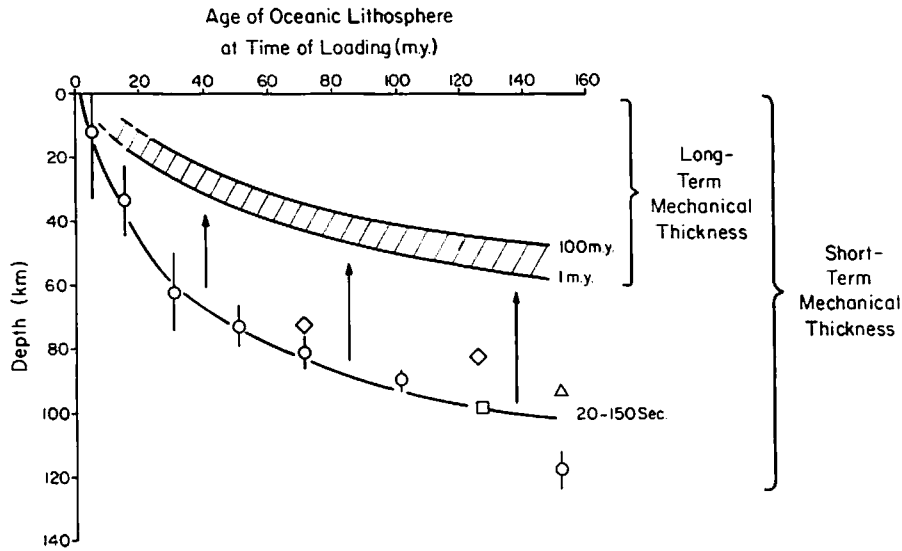


Fig. 13. Schematic diagram indicating our preferred model for the rheology of the oceanic lithosphere for load durations in the region of a few tens of seconds to a few tens of million years. The seismic thickness of the lithosphere is estimated from analysis of surface wave data (Yoshii [1975], triangles; Leeds [1975], circles; Asada and Shimamura [1975], squares; Forsyth [1977], diamonds). Immediately following emplacement of a seamount or oceanic island load the lithosphere relaxes from this short-term mechanical thickness to a long-term mechanical thickness. The equivalent elastic thickness is relatively insensitive to load size and load duration for times greater than 1–10 m.y. The strong dependence of the rheology on temperature results in an increasing effective elastic thickness and rigidity with age.

rigidity and the curvature gives the bending moment of the elastic core, M_e . The total moment and total rigidity are similarly related to curvature as shown by rearranging (4) to give

$$\frac{d^2 w}{dx^2} = -\frac{M_e}{D_e} = -\frac{M}{D} \quad (7)$$

Continuous deflection profiles may be obtained by relating the curvature to the bending moment through (5)–(7) and then numerically solving the appropriate differential (3) and (4).

In order to carry out the integration for bending moment over the vertical stress profile in (5), we modified the yield envelope by fitting the lower thermally dependent yield stress (out to 4 kbar) to a regression line on depth. The regression line has a zero intercept at approximately the mechanical thickness. The effect of neglecting the lower part of the yield envelope remains less than $\approx 3\%$ for a wide range of bending moments. With this modification, the vertical stress profile is defined by three straight lines: the depth-dependent cataclastic yield stress (σ_2 , σ_6 in the notation section), the stress developed in the elastic region, and the straight line fit to the ductile yield stress (σ_4).

For seamount and oceanic island loads we substitute (4) for M in (3), with D a function of x . Equation (3) is then solved by a finite difference technique which, after starting with the elastic solution, iteratively finds new values of $D(x)$ from the deflection solution until convergence is achieved. The assumed boundary conditions are $w'(0) = w'''(0) = 0$ and $w(L) = w'(L) = 0$ where $L = 6\alpha$ (notation section). Convergence to $<1\%$ in $w(x)$ at $x = 0$ is generally achieved within 3–5 iterations.

An alternative numerical technique in which (3) and (7) are solved simultaneously is a fourth-order Runge-Kutta integration [McAdoo et al., 1978; Bodine and Watts, 1979]. Although the Runge-Kutta integration is not as easily adapted to solving deflections caused by distributed surface loads such as seamounts and oceanic islands, it is useful for deflections

seaward of trenches where memory of strain history may be important. Startup boundary conditions for a stepwise integration are required and may be estimated by assuming the plate to be elastic at great distances from the point of loading. The rigidity for this region is determined by the mechanical thickness H . Boundary conditions for the transition from elastic to elastic-plastic rheology (deflection, deflection slope, bending moment, and bending moment slope) are taken from the elastic model at $x = x_{i1}$ (Figure 7). At these points both bending moment and curvature are zero (when $T = 0$), so the vertical distribution of stress for the yield envelope and the elastic model are considered equivalent. Determinations of subsequent boundary conditions for each step of integration toward x_{i2} from x_{i1} are obtained by solving (3) and (4). Solutions using both numerical methods have been compared to analytic solutions for the purely elastic plate and compared to each other for the yield envelope rheology. Results are in agreement to within limits of numerical accuracy.

We note that in a similar calculation using the Runge-Kutta integration by Bodine and Watts [1979] a factor of 4 was omitted in the expression relating curvature and bending moment for the case of depth-dependent yield stress (equation (13) [Bodine and Watts, 1979] should be $\dots 4\sigma_2 \zeta_0$ instead of $\dots \sigma_2 \zeta_0$). The effect of this correction is to slightly weaken the plate and lower the horizontal stresses required to explain observations. The conclusions and discussions of Bodine and Watts [1979] remain unaffected.

The deflection curve for seamount and oceanic island loads can be considered to result from an initial response that relaxes to a relatively unchanging long-term response. We do not consider strain history for this case. The oceanic lithosphere seaward of trenches, however, can be considered to be moving through positions requiring first bending in one direction and then the other. Consideration of strain history is required and is approximated in our model through the use of the Runge-Kutta integration. As long as bending increases, regions which have yielded will continue to behave plastically,

and the elastic core will continue to decrease in thickness (Figure 7). Unbending begins when the bending moment is a maximum (M_0 at $x = x_{r2}$). At this point the lithospheric plate becomes once again entirely elastic. The elastic bending stresses described by the vertical stress profile for this bending moment must be relieved before stresses of the opposite sign can develop and yielding governed by the opposite sides of the yield envelope may occur. This condition is represented in our model by integrating with an 'effective' yield envelope. The effective yield envelope has sides with slopes determined from the sums of the conjugate sides of the original envelope. The top and bottom of the elastic core start once again at the top and bottom of the plate, respectively, as if the bending moment and curvature were zero. Thus the integration is carried out with $M_{eff} = M(x) - M_0$, where M_{eff} is the bending moment value used in the integration for ζ_1 and ζ_2 and $M(x)$ is the actual bending moment represented by the vertical stress distribution. When the elastic core again decreases to the minimum thickness it reached before unbending began, the use of the effective yield envelope is no longer necessary. Evidence of previous strain will have been removed by the more recent bending. Numerical integration continues with the original yield envelope using $M(x)$.

Horizontal forces are applied only for bending at trenches and are assumed orthogonal to the trench. The horizontal force T is applied over the thickness of the plate. Since the yield envelope has zero strength at the upper and lower plate surfaces, yielding occurs immediately even when curvature is zero. The result of yielding due to horizontal forces is a stress concentration in the elastic core. Because of the difference in tensile and compressive brittle shear strengths and the ductile shear strength of our model, more yielding may occur on one side of the plate than on the other. To maintain boundary conditions at $x = x_{r1}$ ($M = 0$, $w'' = 0$), a stress gradient develops in the elastic core which may be considered a result of implicit boundary conditions acting at the bottom of the plate. Strain rates for Outer Rise deflections may be estimated from the convergence rate at the plate boundary. Using a subduction rate of 5 cm/yr and estimates of maximum curvature from observed bathymetry profiles seaward of the Bonin and Mariana trenches, we estimate a maximum strain rate of 10^{-15} s $^{-1}$.

We also point out three other considerations in the modeling studies. (1) The restoring force depends on the density contrast between the infill material and the asthenosphere and most likely is not constant. This will affect the apparent wavelength of deflection. (2) A plate bending under a load does not strain at the same rate everywhere laterally or through a vertical section. Thus the assumption of a constant strain rate for the model is a significant simplification. (3) Errors due to neglect of shear forces in the vertical plane and the assumption of a stress-free neutral surface are believed to be small because dimensions of the plate are large and deflections are generally small (slope <4%).

NOTATION

- w deflection, m.
 E Young's modulus (relaxed), equal to 6.5×10^{10} N/m 2 .
 ν Poisson's ratio, equal to 0.25.
 T_e effective (or equivalent) elastic thickness.
 H mechanical thickness.

- D rigidity, equal to $EH^3/[12(1 - \nu^2)]$ N m.
 ρ_c density of load and sediment infill, equal to 2.6×10^3 kg/m 3 .
 ρ_w density of water, equal to 1.0×10^3 kg/m 3 .
 ρ_m density of asthenosphere, equal to 3.4×10^3 kg/m 3 .
 k restoring force per unit deflection, equal to $g(\rho_m - \rho_c)$ N/m 3 .
 α flexural parameter, equal to $(4D/k)^{1/4}$ m.
 w_b Outer Rise amplitude maximum (for the elastic plate formulation, see *Bodine and Watts* [1979]).
 $M(0)$ bending moment at $x = 0$, equal to $w_b(2kD)^{1/2}e^{-1/4}$ (for the elastic plate formulation, see *Bodine and Watts* [1979]).
 R universal gas constant, equal to 1.98 cal/ $^\circ$ K mol.
 A thickness of thermal lithosphere, equal to 125 km.
 τ_0 time constant for cooling plate model, equal to 62.8 m.y.
 T_0 temperature at base of the thermal lithosphere, equal to 1333 $^\circ$ C.
 σ_2 brittle strength slope (tension), equal to 0.222 bar/m.
 σ_6 brittle strength slope (compression), equal to 0.666 bar/m.
 σ_4 slope of regression line fit to bottom of yield envelope.
 ϵ strain, %.
 $\dot{\epsilon}$ strain rate, s $^{-1}$.
 t load duration which corresponds with the assumed strain rate, calculated using the coefficients from Table 2.
 Q_p activation energy (power law), equal to 122 kcal/mole (dry) and 105 kcal/mol (wet).
 Q_D activation energy (Dorn law), equal to 128 kcal/mol (dry) and 110 kcal/mol (wet).

Acknowledgments. We would like to express appreciation to M. P. Bieniek and Lembitt Kutt of Civil Engineering Department, Columbia University, for guidance and assistance in formulating the model and to W. Menke for collaboration in the construction of the iterative finite difference technique. We thank T. E. Endo for providing a preprint of his paper. We also thank W. Haxby, J. Cochran, G. Karner, and S. Daly for helpful discussion and comments. This work was supported by National Science Foundation grant OCE 79-18917 and Office of Naval Research contract N-00014-80-C-0098 Scope I. Lamont-Doherty Geological Observatory contribution 3137.

REFERENCES

- Anderson, D. L., and J. B. Minster, Seismic velocity, attenuation and rheology of the upper mantle, Prof. Jean Coulomb Symposium on Source Mechanism and Earthquake Prediction, *Ann. Phys.*, 1980.
 Apple, R. A., and G. A. McDonald, The rise in sea level in contemporary times at Honaunau, Kona, Hawaii, *Pac. Sci.*, 20, 125-136, 1966.
 Asada, T., and H. Shimamura, A structure of the oceanic lithosphere as revealed by ocean-bottom seismography, paper presented at the Interdisciplinary Symposia, 16th General Assembly, Intl. Union of Geod. and Geophys., Grenoble, 1975.
 Ashby, M. F., and R. A. Verrall, Micromechanisms of flow and fracture, and their relevance to the rheology of the upper mantle, *Philos. Trans. R. Soc. London, Ser. A*, 288, 59-95, 1978.
 Barrell, J., The strength of the Earth's crust, *J. Geol.*, 22, 729-741, 1914.
 Bodine, J. H., and A. B. Watts, Lithospheric flexure seaward of the Bonin and Mariana trenches, *Earth Planet. Sci. Lett.*, 43, 132-148, 1979.
 Brace, W. F., and D. L. Kohlstedt, Limits on lithospheric stress imposed by laboratory experiments, *J. Geophys. Res.*, 85, 6248-6252, 1980.
 Caldwell, J. G., The mechanical behavior of the oceanic lithosphere

- near subduction zones, Ph.D. thesis, 151 pp., Cornell Univ., Ithaca, N. Y., 1979.
- Caldwell, J. G., W. F. Haxby, D. E. Karig, and D. L. Turcotte, On the applicability of a universal elastic trench profile, *Earth Planet. Sci. Lett.*, **31**, 239, 1976.
- Cazenave, A., B. Lago, K. Dominti, and K. Lambeck, On the response of the ocean lithosphere to seamount loads from GEOS 3 satellite radar altimeter observations, *Geophys. J. R. Astron. Soc.*, **63**, 233–254, 1980.
- Chapple, W. M., and D. W. Forsyth, Earthquakes and bending of plates at trenches, *J. Geophys. Res.*, **84**, 6729–6749, 1979.
- Chen T., and D. W. Forsyth, A detailed study of two earthquakes seaward of the Tonga Trench: Implications for mechanical behavior of the oceanic lithosphere, *J. Geophys. Res.*, **83**, 4995–5004, 1978.
- Clague, D. A., and R. D. Jarrard, Tertiary Pacific plate motion deduced from the Hawaiian-Emperor Chain, *Geol. Soc. Am. Bull.*, **84**, 1135–1154, 1973.
- Cochran, J. R., An analysis of isostasy in the world's oceans, 2, Mid-ocean ridge crests, *J. Geophys. Res.*, **84**, 4713–4729, 1979.
- Crough, S. T., and G. A. Thompson, Numerical and approximate solutions for lithospheric thickening and thinning, *Earth Planet. Sci. Lett.*, **31**, 397–402, 1976.
- DeBremaecker, J.-C., Is the oceanic lithosphere elastic or viscous?, *J. Geophys. Res.*, **82**, 2001–2004, 1977.
- Detrick, R. S., and T. S. Crough, Island subsidence, hot spots, and lithospheric thinning, *J. Geophys. Res.*, **83**, 1236–1244, 1978.
- Detrick, R. S., and A. B. Watts, An analysis of isostasy in the world's oceans, 3, Aseismic ridges, *J. Geophys. Res.*, **84**, 3637–3653, 1979.
- Dubois, J., J. Launay, and J. Recy, Some new evidence on lithospheric bulges close to island arcs, *Tectonophysics*, **26**, 189, 1975.
- Endo, T. E., and D. B. Rogers, Focal mechanisms for upper mantle earthquakes and flexure of the lithosphere near Hawaii, submitted to *J. Geophys. Res.*, 1981.
- Engdahl, E. R., and C. H. Scholz, A double Benioff Zone beneath the central Aleutians: An unbending of the lithosphere, *Geophys. Res. Lett.*, **4**, 473–476, 1977.
- Forsyth, D. W., The evolution of the upper mantle beneath mid-ocean ridges, *Tectonophysics*, **38**, 89–118, 1977.
- Gass, I. G., R. Thorpe, H. N. Pollack, and D. S. Chapman, Geological and geophysical parameters for mid-plate volcanism (abstract), *Eos Trans. AGU*, **58**, 503, 1977.
- Goetze, C., The mechanisms of creep in olivine, *Philos. Trans. R. Soc. London, Ser. A*, **288**, 99–119, 1978.
- Goetze, C., and W. F. Brace, Laboratory observations of high-temperature rheology of rocks, *Tectonophysics*, **13**, 583–600, 1972.
- Goetze, C., and B. Evans, Stress and temperature in the bending lithosphere as constrained by experimental rock mechanics, *Geophys. J. R. Astron. Soc.*, **59**, 463–478, 1979.
- Gunn, R., A quantitative study of the lithosphere and gravity anomalies along the Atlantic Coast, *J. Franklin Inst.*, **237**, 139–154, 1944.
- Hanks, T. C., The Kuril Trench-Hokkaido Rise system: Large shallow earthquakes and simple models of deformation, *Geophys. J. R. Astron. Soc.*, **23**, 173–189, 1971.
- Hasegawa, A., N. Umino, and A. Takagi, Double planed structure of the deep seismic zone in the northeastern Japan arc, *Tectonophysics*, **47**, 43–58, 1977.
- Houtz, R., C. Windisch, and S. Murauchi, Changes in the crust and upper mantle near the Japan-Bonin Trench, *J. Geophys. Res.*, **85**, 267–274, 1980.
- Kohlstedt, D. L., and C. Goetze, Low-stress high-temperature creep in olivine single crystals, *J. Geophys. Res.*, **79**, 2045–2051, 1974.
- Kohlstedt, D. L., C. Goetze, and W. B. Durham, Experimental deformation of single crystal olivine with application to flow in the mantle, in *Physics and Chemistry of Rocks and Minerals*, pp. 35–41, John Wiley, New York, 1976.
- Leeds, A. R., Lithospheric thickness in the western Pacific, *Phys. Earth Planet. Inter.*, **11**, 61–64, 1975.
- McAdoo, D. C., J. G. Caldwell, and D. L. Turcotte, On the elastic-perfectly plastic bending of the lithosphere under generalized loading with application to the Kuril Trench, *Geophys. J. R. Astron. Soc.*, **54**, 11–26, 1978.
- McDougall, I., and Aziz-ur-Rahman, Age of the Gauss-Matuyama boundary and of the Kaena and Mammoth Events, *Earth Planet. Sci. Lett.*, **14**, 367–380, 1972.
- McDougall, I., and D. A. Swanson, Potassium-argon ages of lavas from the Hawaii and Pololu volcanic series, Kohala volcano, Hawaii, *Bull. Geol. Soc. Am.*, **83**, 3831–3838, 1972.
- McKenzie, D. P., and C. Bowin, The relationship between bathymetry and gravity in the Atlantic ocean, *J. Geophys. Res.*, **81**, 1903–1915, 1976.
- McNutt, M., Compensation of oceanic topography: An application of the response function technique to the Surveyor area, *J. Geophys. Res.*, **84**, 7589–7598, 1979.
- McNutt, M., and H. W. Menard, Lithospheric flexure and uplifted atolls, *J. Geophys. Res.*, **83**, 1206–1212, 1978.
- Moore, J. G., Relation between subsidence and volcanic load, Hawaii, *Bull. Volcanol.*, **34**, 562–575, 1970.
- Parsons, B., and J. G. Sclater, An analysis of the variation of ocean floor bathymetry and heat flow with age, *J. Geophys. Res.*, **82**, 803–827, 1977.
- Post, R. L., High temperature creep of Mt. Burnet dunite, *Tectonophysics*, **42**, 75–110, 1977.
- Stocker, R. L., and M. F. Ashby, On the rheology of the upper mantle, *Rev. Geophys. Space Phys.*, **11**, 391–426, 1973.
- Suyenaga, W., Earth deformation in response to surface loading: Application to the formation of the Hawaiian Ridge, Ph.D. thesis, 147 pp., Univ. of Hawaii, Honolulu, 1977.
- Swanson, D. A., Magma supply rate at Kilanea volcano, 1952–1971, *Science*, **175**, 169–170, 1972.
- Vening-Meinesz, F. A., Gravity over the Hawaiian Archipelago and over the Madiera Area: Conclusions about the Earth's crust, *Proc. K. Ned. Akad. Wet.*, **44**, 1–12, 1941.
- Walcott, R. I., Flexural rigidity, thickness, and viscosity of the lithosphere, *J. Geophys. Res.*, **75**, 3941–3954, 1970.
- Walcott, R. I., Past sea levels, eustasy and deformation of the Earth, *Quaternary Res.*, **2**, 1–14, 1972.
- Watts, A. B., An analysis of isostasy in the world's oceans, 1, Hawaiian-Emperor seamount chain, *J. Geophys. Res.*, **83**, 5889–6004, 1978.
- Watts, A. B., and J. R. Cochran, Gravity anomalies and flexure of the lithosphere along the Hawaiian-Emperor seamount chain, *Geophys. J. R. Astron. Soc.*, **38**, 119–141, 1974.
- Watts, A. B., and M. Talwani, Gravity anomalies seaward of deep-sea trenches and their tectonic implications, *Geophys. J. R. Astron. Soc.*, **36**, 57–90, 1974.
- Watts, A. B., J. R. Cochran, and G. Selzer, Gravity anomalies and flexure of the lithosphere: A three-dimensional study of the Great Meteor Seamount, Northeast Atlantic, *J. Geophys. Res.*, **80**, 1391–1398, 1975.
- Watts, A. B., J. H. Bodine, and N. R. Ribe, Observations of flexure and the geologic evolution of the Pacific ocean basin, *Nature*, **238**, 532–537, 1980a.
- Watts, A. B., J. H. Bodine, and M. S. Steckler, Observations of flexure and the state of stress in the oceanic lithosphere, *J. Geophys. Res.*, **85**, 6369–6376, 1980b.
- Weertman, J., and J. R. Weertman, High-temperature creep of rock and mantle viscosity, *Annu. Rev. Earth Planet. Sci.*, **3**, 293–316, 1975.
- Withjack, M., A convective heat transfer model for lithospheric thinning and crustal uplift, *J. Geophys. Res.*, **84**, 3008–3022, 1979.
- Yoshii, T., Regionality of group velocities of Rayleigh waves in the Pacific and the thickening of the plate, *Earth Planet. Sci. Lett.*, **25**, 305–312, 1975.

(Received September 22, 1980;
revised December 29, 1980;
accepted December 31, 1980.)